Faraday Discuss. Chem. Soc., 1982, **73**, 205–220

The He–N_2 Anisotropic Van der Waals Potential

Test of a Simple Model Using State-to-state Differential Scattering Cross-sections

BY MANFRED FAUBEL, KARL-HEINZ KOHL AND J. PETER TOENNIES

Max-Planck-Institut für Stromungsforschung,
3400 Gottingen, West Germany

AND KWONG TIN TANG AND YAT YAN YUNG
Department of Physics, Pacific Lutheran University,
Tacoma, Washington 98447, U.S.A.

Received 3rd December, 1981

For He–N_2 the total and the $j = 0 \rightarrow 2$, $1 \rightarrow 3$ rotationally inelastic differential cross-sections have been measured at a collision energy of $E_{cm} = 27.3$ meV and at centre-of-mass angles between 5 and 50°. These new data have been used to test the validity of an anisotropic potential recently calculated using the model of Tang and Toennies. Theoretical close-coupling cross-sections based on the potential are found to be in good agreement with the data. By studying the effect of small modifications in the potential it has been possible to estimate that the model potential predicts the anisotropy with only a negligible error but understimates the well depth of the spherical potential by *ca.* 20%.

INTRODUCTION

The anisotropy of molecular potentials is of great interest for an understanding of crystal structure [1] and also the solid, liquid and gaseous equations of state.[2] The anisotropy of molecules also has a direct effect on gas dynamic transport coefficients and rotational relaxation times.[2] Recently developed molecular-beam experiments of essentially two types, in which (1) the cross-section anisotropy of polarized molecule beams [3] and (2) the rotationally inelastic differential cross-sections are measured,[4] have made possible a precise measurement of the anisotropy of the Van der Waals potential. The latter experiments, first successfully carried out for TlF in small angle collisions,[5] have since been extended to larger scattering angles, first for Li^+–H_2,[6] H^+–H_2 [7] and then for He–H_2, Ne–H_2 collisions [8] using time-of-flight techniques. These scattering experiments have made it possible critically to test *ab initio* CI calculations of anisotropic Van der Waals potentials. They have also stimulated the development of semi-classical [9] and semi-empirical [10] models, which rely only on easily calculated asymptotic interaction parameters. For the rare-gas–H_2 systems the model of Tang and Toennies [9] has been able to predict not only the anisotropy for He–H_2 and Ne–H_2,[11] but also the full potential hypersurface in good agreement with all of the available *ab initio* and experimental data.

Unfortunately, until recently [13] beam experiments were not available to test the model for more typical molecules.

In this paper we report on extensive measurements of the He–N_2 rotationally inelastic differential cross-sections at $E_{cm} = 27.3$ meV in the range of centre-of-mass scattering angles 5-50°.[14] Parallel to this development it has also recently been

possible to apply the Tang–Toennies model to calculate the anisotropic Van der Waals potential of He–N_2.[15] In the present paper we report on a comparison of inelastic differential cross-sections calculated for the model potential with the new experimental data. The overall agreement is good and well within the errors of the input parameters. The small remaining differences between the model potential and the true potential are estimated.

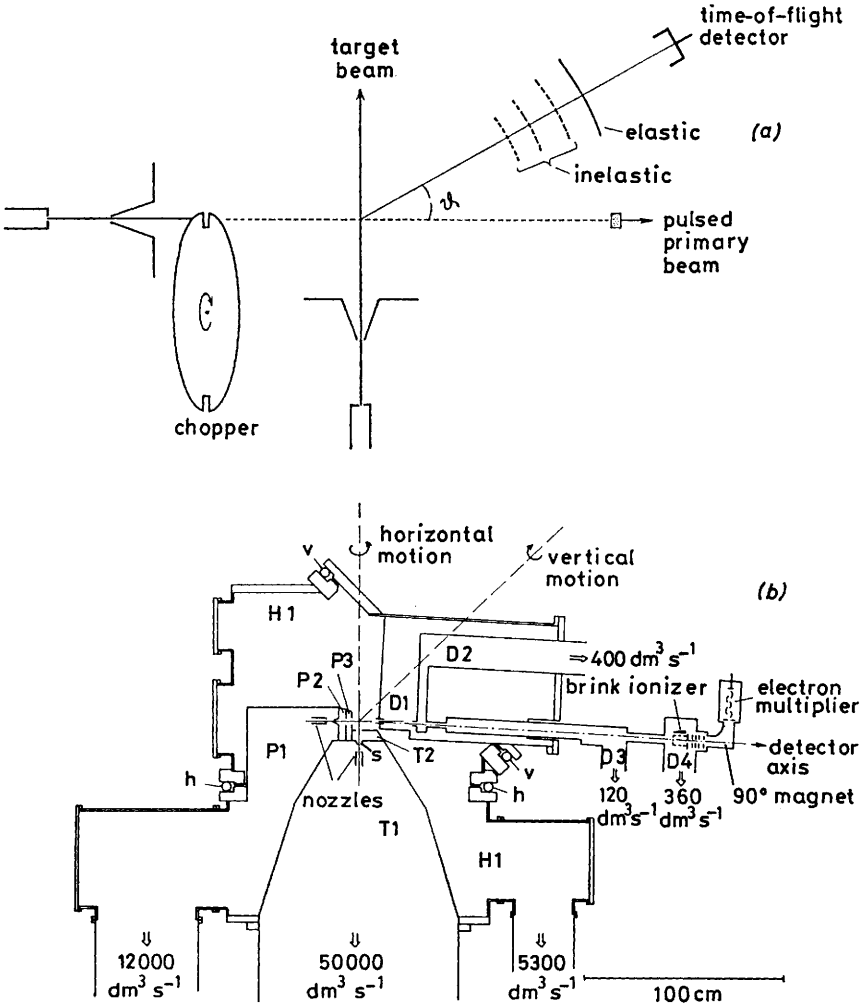

FIG. 1.—(*a*) The principle of the crossed supersonic molecular beams time-of-flight apparatus shown schematically. (*b*) The actual design of the machine, incorporating six differential pumping stages for the production of two well defined supersonic beams. A helium partial pressure of 10^{-16} Torr in the mass-spectrometer detector is sustained by four additional differential vacuum stages. Horizontal and vertical scattering angles are selected by motion of the ball bearing supported flanges "v" and "h." The flight-path length of 165 cm allows 1% velocity resolution.

EXPERIMENTAL

APPARATUS

The apparatus is shown schematically in fig. 1(*a*) and to scale in the side view machine assembly drawing in fig. 1(*b*). Two nearly monochromatic molecular beams, a He primary and the N_2 target beam, are formed in nozzle expansions. After collimation by skimmers and additional differentially pumped collimators the two beams intersect at the centre of the apparatus. Scattered He atoms are observed by the mass-spectrometer detector at the right-hand side of fig. 1(*a*) or (*b*), respectively. The scattering angle is changed by rotating the detector part of the machine with respect to the vertical axis indicated in fig. 1(*b*). For observing individual rotational transitions at a given scattering angle the flight time, and thus the energy change of scattered molecules, is measured. To do this a 12 cm diameter chopper wheel with four 1 mm wide slots is rotated through the He beam at 24 000 r.p.m. The count rate of scattered particles arriving at the detector is then recorded as a function of the time delay from the passage of a chopper slit through the helium beam. A typical time-of-flight spectrum is shown in fig. 2. The time resolution and thus the energy-level resolution is limited by apparatus effects such as the finite chopper opening time of 7 μs and the ratio of the ionizer length $\Delta L \approx 1.5$ cm to the length of the total flight path, which is $L = 165$ cm and thus allows a velocity resolution of 1% corresponding to an energy resolution of 0.6 meV at a He energy of 30 meV. A second, and more serious, kinematical limitation on the energy resolution [4] results from the finite velocity spreads and angular divergences of the colliding beams. Hence, the scattering experiment was optimized in the sense of chap. IV.B of ref. (4). The actual beam distributions of the present experiment, which are either affecting the resolution or the evaluation of the scattering experiment, are, for brevity, all summarized in table 1. At $\theta_{LAB} = 20°$ the resulting overall energy resolution is 0.8 meV for a collision energy of 27 meV.

TABLE 1.—EXPERIMENTAL PARAMETERS

component	nozzle conditions	spreads (f.w.h.m.)
helium primary beam	pressure: $p_0 = 100$ bar diameter: $D_N = 20$ μm temp.: $T_0 = 88$ K	velocity: $\Delta v/v_0 = 0.7\%$ at $v_0 = 950$ m s^{-1} angular: $\Delta\alpha = 0.75°$ in-plane $\Delta\beta = 2.0°$ out-of-plane
N_2 target beam	pressure: $p_0 = 8$ bar diameter: $D_N = 100$ μm temp.: $T_0 = 300$ K	velocity: $\Delta v/v_0 = 5\%$ at $v_0 = 750$ m s^{-1} angular: $\Delta\alpha = 2°$ $\Delta\beta = 2°$ rotational population [ref. (16)] $j_i = 0 : 52\%$ $j_i = 1 : 33\%$ $j_i = 2 : 15\%$
detector	./.	velocity: $\Delta v/v = \Delta L/L = 1\%$ at $L = 165$ cm angular: $\Delta\alpha = 0.4°$ $\Delta\beta = 0.2°$

The narrow beam collimation and the long flight path lead to a drastic loss in scattering intensity. Therefore, the He partial pressure in the detector had to be lowered to less than the signal density of 10^{-16} Torr. As shown in fig. 1(*b*) the detector vacuum is sustained against the main chamber pressure of 10^{-6} Torr by four differential pumping stages along the flight path. With an estimated He detection efficiency of 10^{-5} the average detector count rate was *ca.* 10 counts s^{-1} and measuring times of typically 10 to 30 h were required to obtain the TOF spectra shown in fig. 2 and 3.

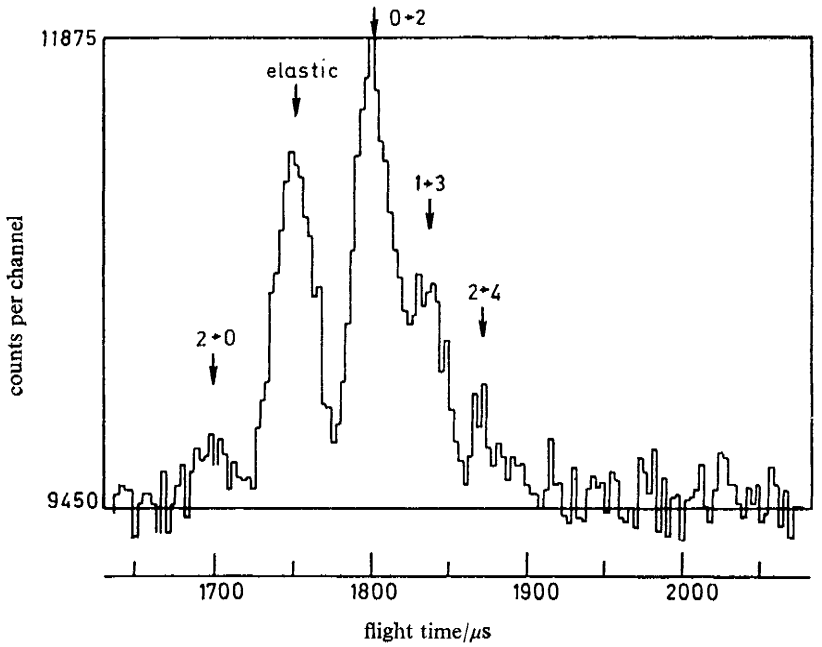

FIG. 2.—Example of a time-of-flight spectrum of He scattered from N_2. The spectrum was accumulated in a measuring time of 14 h. For the collision energy of $E_{cm} = 27.3$ meV and the scattering angle $\theta_{LAB} = 20°$ (equivalent to $\vartheta_{cm} = 17.5°$) the flight time of elastically scattered He is 1750 μs. Well separated from the elastic peak He which has excited the $j_i = 0$ to $j' = 2$ rotational transition of N_2 and lost an energy of 1.5 meV (12 cm^{-1}) arrives at a flight time of 1800 μs. Additional inelastic peaks from the 1→3, 2→0 and 2→4 rotational transitions are also observed as indicated by the arrows.

CROSS-SECTION MEASUREMENTS

With the He and N_2 beam velocities listed in table 1 the centre-of-mass collision energy is $E_{cm} = 27.3$ meV An example of a TOF spectrum measured at a laboratory scattering angle of 20° is shown in fig. 2. It shows a fast peak of elastically scattered helium atoms at a flight time of 1750 μs. At 1800 μs an even larger second peak is found with an energy loss of 1.5 meV equal to the level spacing between the $j = 0$ and the $j = 2$ rotational levels of *ortho*-N_2. The shoulder on the right-hand side of the 0→2 transition peak results from the 1→3 transition of *para*-N_2. Also observed, and indicated by the arrows in fig. 2, are the much weaker 2→0 and 2→4 rotational transitions of the $j_i = 2$ state of *ortho*-N_2, which, as listed in table 1, accounts for 15% of all N_2 beam molecules. Higher rotational transitions could not be observed and are estimated to have transition probabilities of $< 3\%$ in all measured TOF spectra.

The variation of TOF spectra with scattering angle is shown in fig. 3 for a number of out-of-plane laboratory scattering angles in the range from 16 to 47°. At most angles the 0→2 and 1→3 rotational transition probabilities are quite small, of the order to 10 to 20%. However, at certain specific angles $\theta_{LAB} = 20$, 28 and 47° and at larger angles the inelastic transition probabilities are comparable to the elastic probabilities.

Using the N_2 initial rotational state populations of table 1 the TOF spectra were corrected to yield state-to-state differential laboratory cross-sections. These were then transformed into the centre-of-mass system and are shown in fig. 4 as the total and the 0→2 and 1→3 rotationally inelastic differential cross-sections. The systematic average error in the absolute calibration in $Å^2\ sr^{-1}$ is estimated to be 5%. The accuracy of the scattering angles is 0.2°.

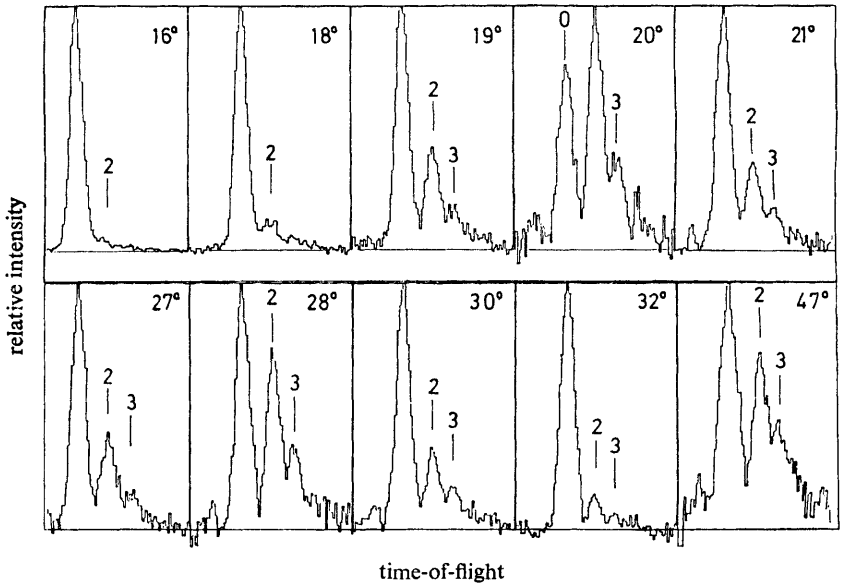

FIG. 3.—He–N_2, E_{cm} = 27.3 meV time-of-flight spectra at various laboratory scattering angles. Here the amplitude of the largest peak is normalized to unity. Locations of the 0→2 and 1→3 rotational transitions are labelled by vertical lines.

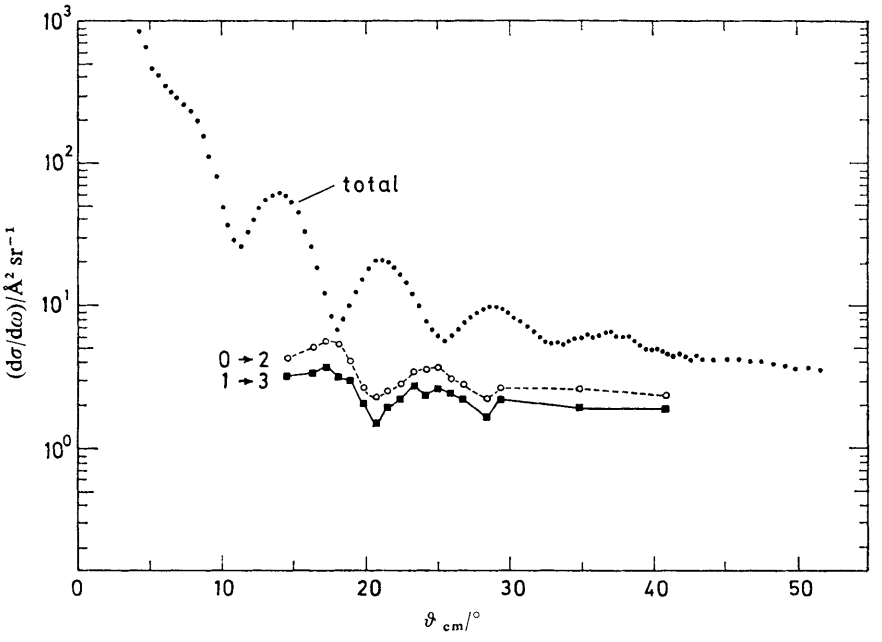

FIG. 4.—Experimental centre-of-mass total (●), 0→2 (○) and 1→3 (■) rotationally inelastic cross-sections for He–N_2 at E_{cm} = 27.3 meV.

Individual points have statistical errors of *ca.* 10% for cross-sections <5 Å^2 sr^{-1} and 3% for larger cross-sections.

All cross-sections show very well resolved Fraunhofer diffraction oscillations, but as an indication of the very shallow well of the He–N_2 potential no characteristic rainbow structure is present. The absolute amplitude of the oscillations in the rotationally inelastic $0\rightarrow2$ and $1\rightarrow3$ transitions is slightly quenched as compared with the total differential cross-section. The $1\rightarrow3$ transition differential cross-section is smaller than the $0\rightarrow2$ cross-section, and its oscillatory structure is almost proportional to the $0\rightarrow2$ cross-section with the proportionality ratio of *ca.* 0.7. This value agrees to within 10% with the ratio predicted by the infinite-order sudden factorization rule.[14] Remarkably, however, the total cross-section oscillations are shifted almost exactly 180° out-of-phase with respect to the inelastic cross-sections.

THEORETICAL

THE POTENTIAL MODEL

The He–N_2 Van der Waals interaction potential used to fit the data is reported in ref. (15) and was calculated from the potential model described in ref. (9) and (11). This model potential is in some respects similar to the Buckingham potential and related models proposed in the past. In keeping with these, the short-range potential is assumed to be of the Born–Mayer form, with potential parameters, however, determined from an accurate SCF calculation. The long-range potential is given by the usual perturbation expansion of which all the terms are included. However, the asymptotic divergence of the full expansion is accounted for in a simple approximate fashion. In the intermediate region a new term is introduced to account for the perturbation of the dispersion forces by the repulsion.

The dispersion coefficients can be accurately expressed in terms of integrals over the frequencies of the dynamic multipole polarizabilities of the isolated partners. The dynamic polarizability for He was derived from accurate CI calculations.[17] For N_2 they have been estimated by an SCF procedure.[18] For the explicit form of the rather lengthy integrals over the appropriate combinations of dynamic polarizabilities which give the dispersion coefficients we refer to ref. (15) and (18). The long-range dispersion potential is expanded in R, the distance between centres-of-mass,

$$V_{\mathrm{Disp}}(R,\gamma) = -\sum_{n\geqslant 3} f_{2n}(R,\gamma)\frac{C_{2n}(\gamma)}{R^{2n}} \qquad (1)$$

where γ is the angle between R and the molecular axis. To account for the anisotropy the $C_{2n}(\gamma)$ are expanded in Legendre functions up to P_4

$$C_{5n}(\gamma) = C^{\circ}_{2n}[1 + \Gamma^{(2)}_{2n}P_2(\cos\gamma) + \Gamma^{(4)}_{2n}P_4(\cos\gamma)]. \qquad (1a)$$

The numerical values of the C°_{2n} and $\Gamma^{(k)}_{2n}$ are listed in table 2. To remove the asymp-

TABLE 2.—SOME OF THE DISPERSION COEFFICIENTS C°_{2n} AND $\Gamma^{(k)}_{2n}$ VALUES USED FOR CALCULATING THE LONG-RANGE He–N_2 POTENTIAL [15]

term	C°_{2n}/a.u. [a]	$\Gamma_{2n}{}^{(2)}$	$\Gamma_{2n}{}^{(2)}$
$2n = 6$	10.2	0.101	0
$2n = 8$	185	0.486	−0.045
$2n = 10$	4 360	0.486	−0.045
$2n = 12$	13 3519	0.486	−0.045

[a] 1 a.u. = 0.529 Å (length); 1 a.u. = 27.21 eV (energy).

totic divergence of the dispersion series each of the terms $C_{2n}(\gamma)/R^{2n}$ has been truncated by a function:

$$f_{2n}(R,\gamma) = \begin{cases} 1 & \text{for } R > \rho_{2n} \quad = \sqrt{\dfrac{C_{2n+2}(\gamma)}{C_{2n}(\gamma)}} \\ \dfrac{R-\rho_{2n-2}}{\rho_{2n}-\rho_{2n-2}} & \text{for } \rho_{2n-2} \leqslant R \leqslant \rho_{2n} \\ 0 & \text{for } R < \rho_{2n-2} = \sqrt{\dfrac{C_{2n}(\gamma)}{C_{2n-2}(\gamma)}}. \end{cases} \tag{2}$$

The repulsive part of the He–N_2 potential was obtained by calculating the SCF potential energies in the range $4 \leqslant R/\text{a.u.} \leqslant 8$ for the orientation angles $\gamma = 0$, 45 and 90°.[15] The SCF energy values were also fitted to a 3-term Legendre expansion in γ, each coefficient of which could be well approximated by Born–Mayer radial functions:

$$V_{\text{SCF}}(R,\gamma) = \sum_{\gamma=0}^{2} A_{2\lambda}\exp(-\beta_{2\lambda}R)P_{2\lambda}(\cos\gamma) \tag{3}$$

with the values $A_{2\lambda}$ and $\beta_{2\lambda}$ being given in table 3.

TABLE 3.—SCF BORN–MAYER RADIAL POTENTIAL VALUES $A_{2\lambda}$ AND $\beta_{2\lambda}$ FOR He–N_2 [15]

term	$A_{2\lambda}$/a.u.	$\beta_{2\lambda}$/a.u.
$2\lambda = 0$	134.7	2.094
$2\lambda = 2$	217.9	2.122
$2\lambda = 4$	91.86	2.178

These two asymptotic regions of the He–N_2 potential are joined together by the following prescription which takes account of the effect of electron overlap on the dispersion coefficients. This correction has been estimated semi-classically from the energy splitting induced in Drude model molecules when coupled to each other by the SCF interaction:[9]

$$V_{\text{corr}}(R,\gamma) = [M(\text{He}) + M(\text{N}_2)]\left[\left(\frac{\partial^2}{\partial R^2} + \frac{2}{R}\frac{\partial}{\partial R}\right)V_{\text{SCF}}(R,\gamma)\right]. \tag{4}$$

Here the derivatives with respect to R are taken for the SCF potential eqn (3). The factors M (He) and M (N_2) stand essentially for the quotient ω_0/k of the frequency ω_0 and the force constant k of the Drude electron gas model employed for the isolated He and N_2 molecules. Their values can be determined from the known C_6 constants of the He–He and the N_2–N_2 potential, the static polarizabilities of He and of N_2 and the (Drude model) effective number of electrons. The value of M for He [9] is $M(\text{He}) = 0.044$, and for N_2 it was found to be almost independent of the orientation angle γ with an average value of M (N_2) = 0.130.[15]

With this correction the complete model potential reads:

$$V(R,\gamma) = V_{\text{SCF}}(R,\gamma) + V_{\text{corr}}(R,\gamma) + V_{\text{Disp}}(R,\gamma). \tag{5}$$

For computational purposes the standard Legendre representation:

$$V(R,\gamma) = v_0(R) + v_2(R)P_2(\cos\gamma) + v_4(R)P_4(\cos\gamma) + \ldots \tag{5a}$$

was used, and the first three radial potential functions $v_{2\lambda}(R)$ for the He–N_2 interaction are shown in fig. 5 as smooth lines.

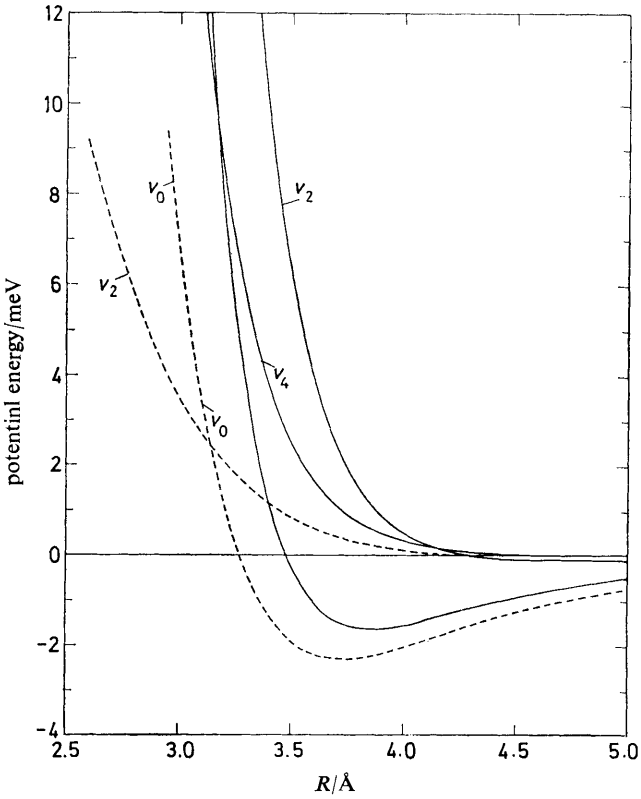

FIG. 5.—Radial terms v_0, v_2 and v_4 of the He–N_2 Van der Waals potential as predicted by the Tang–Toennies potential model (smooth lines). Also shown (dashed lines) are the v_0 and v_2 terms of an experimental He–N_2 potential obtained by Keil, Slankas and Kuppermann from fitting total differential cross-sections only.

The spherical part v_0 of this potential has a well depth of $\varepsilon^\circ = 1.62$ meV and an $R_m^\circ = 3.83$ Å. Remarkably, in the region of the repulsive barrier the $v_2(R)$ potential term is considerably larger than the spherical term while the v_4 term has only a significant effect in the potential well region and at the beginning of the repulsive barrier. For comparison, in fig. 5 we also show (dashed lines) the v_0 and the v_2 term of a recently published He–N_2 potential derived by Keil, Slankas and Kuppermann [19] entirely from total differential cross-section measurements at $E_{cm} = 64$ meV. This potential is an " effective " potential for the total differential cross-section in that it accounts indirectly for the quenching due to inleastic processes. There is a surprisingly large discrepancy between the spherical part v_0 of this previous potential and the v_0 part of the present potential model, which we will discuss later.

COMPUTATION OF CROSS-SECTIONS

Differential elastic and rotationally inelastic cross-sections were computed from this predicted He–N_2 interaction potential for comparison with the experimental

data. The experimental collision energy of $E_{cm} = 27.3$ meV was low enough for a close-coupling calculation including 5 rotational states with 25 coupled channels to give fully converged cross-sections. For the details of the essentially exact quantum close-coupling procedure we refer to ref. (20) or to the review article in ref. (21).

Since the N_2 molecular beam used in the scattering experiments contained both

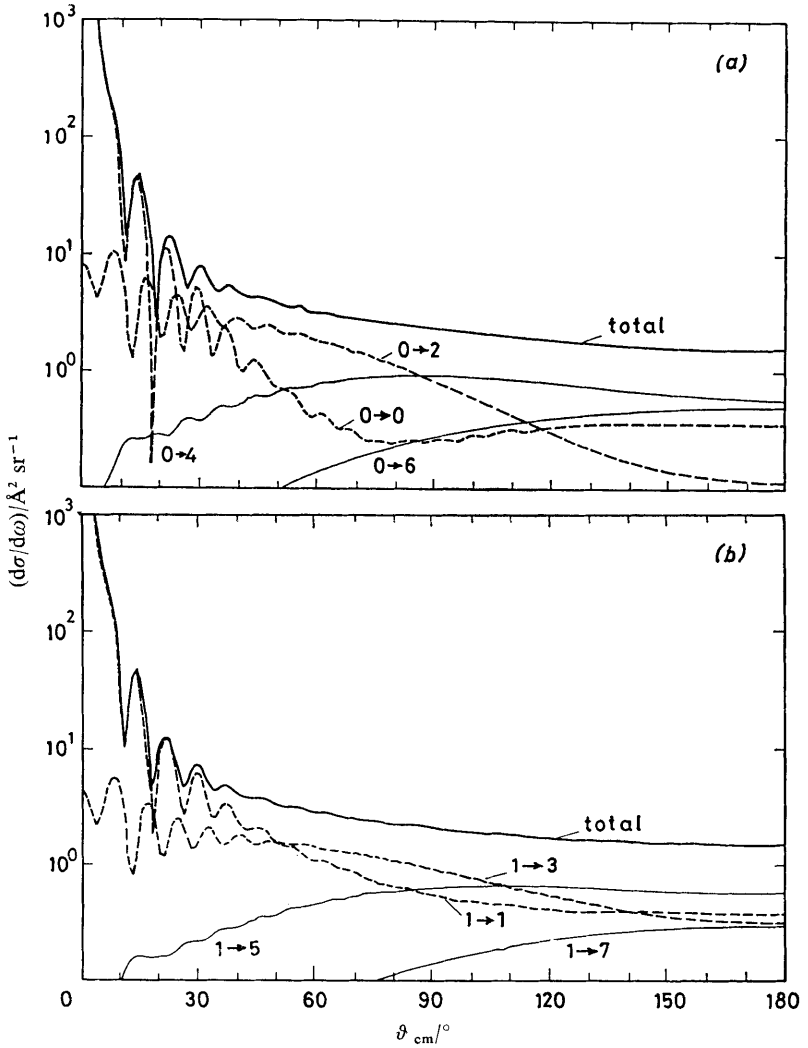

FIG. 6.—5 states, 25 channels close-coupling elastic, rotationally inelastic and total differential cross-sections calculated from the Habitz, Tang and Toennies potential for He–N_2 at $E_{cm} = 27.3$ meV. The initial rotational stage of N_2 is (*a*) $j_i = 0$ and (*b*) $j_i = 1$.

ortho-($j_i = 0,2$) and *para*-($j_i = 1$)N_2, with the populations given in table 1, cross-section calculations had to be performed for the initial states $j_i = 0,1$ and 2. Fig. 6(*a*) and (*b*) show these theoretical cross-sections for the dominant N_2 fractions $j_i = 0$ and $j_i = 1$, respectively, and for the full angular range from $\vartheta_{cm} = 0$ to 180°. Convergence of the calculations was checked at every 10th partial wave by a 64 channel calculation. Additionally, 4 channel (2 states) calculations showed only minor changes

in the cross-sections of 10% in the experimentally important region from 0 to 60°. In further test calculations it was also found that the v_4 term of the potential influences the cross-sections by $<10\%$ for angles $\vartheta < 60°$. The cross-sections shown in fig. 6 are therefore believed to converge also with respect to the potential expansion.

At small scattering angles, up to *ca.* 50°, the elastic and $\Delta j = 2$ rotational transitions are largest, and show the characteristic diffraction oscillations of the experiment. For larger angles the higher $\Delta j = 4$ and $\Delta j = 6$ cross-sections become prevalent, thus giving rise to the rotational rainbow phenomenon observed in Na_2 + rare-gas [22,23] collisions. Also shown in fig. 6 are the total differential cross-sections for $j_i = 0$ and $j_i = 1$. Compared with the rather large differences seen between the individual Δj, and in particular in the $\Delta j = 0$ elastic transitions of the different initial states, the total cross-sections are almost identical for $j_i = 0, j_i = 1$ and also for the $j_i = 2$ state which is not shown here explicitly.

DISCUSSION

COMPARISON OF THEORY AND EXPERIMENT

For the comparison with the measurements, shown in fig. 7, it was more convenient to compare the inelastic 0→2 and 1→3 and the total cross-section. Examination

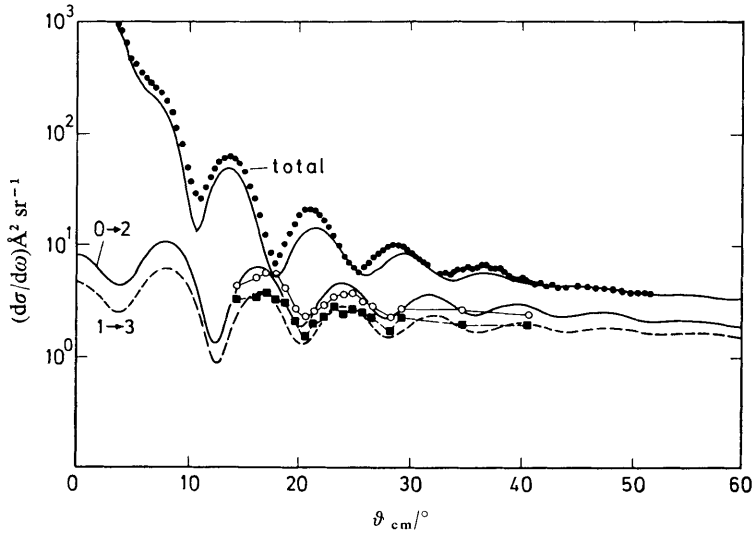

FIG. 7.—Comparison of the predicted theoretical (smooth curves) with the measured total (●), 0→2 (○) and 1→3 (■) differential cross-sections for He–N_2 at $E_{cm} = 27.3$ meV.

of fig. 7 reveals that all characteristic features of the experimental cross-sections, *e.g.* oscillatory decreasing total cross-sections, amplitude of inelastic cross-sections and relative phase shift between the diffraction oscillations of the total and the rotationally inelastic cross-sections, are well predicted by the theory. However, slight deviations exist in the absolute magnitude and in the position of the diffraction maxima.

Part of this discrepancy might arise from the small experimental averaging of the cross-sections over a finite range of centre-of-mass energies and scattering angles. The effect of this convolution of the apparatus resolution with the ideal theoretical cross-section is considered separately in fig. 8. Here, for numerical simplicity, the

" total " differential cross-section generated from an effective spherical potential for $He–N_2$ [19] was used and was convoluted both with the experimental centre-of-mass scattering angle and the energy resolution function. This centre-of-mass resolution function was approximated by a two-dimensional Gaussian distribution with the vacancies in E_{cm} and ϑ_{cm}, and their covariance calculated [4] from the half widths of the molecular-beam spreads and the detector aperture angles given in table 1. The comparison of the convoluted (smooth line) with the original (dashed line) total cross-section at $E_{cm} = 27.3$ meV in fig. 8 shows a considerable quenching only in the region

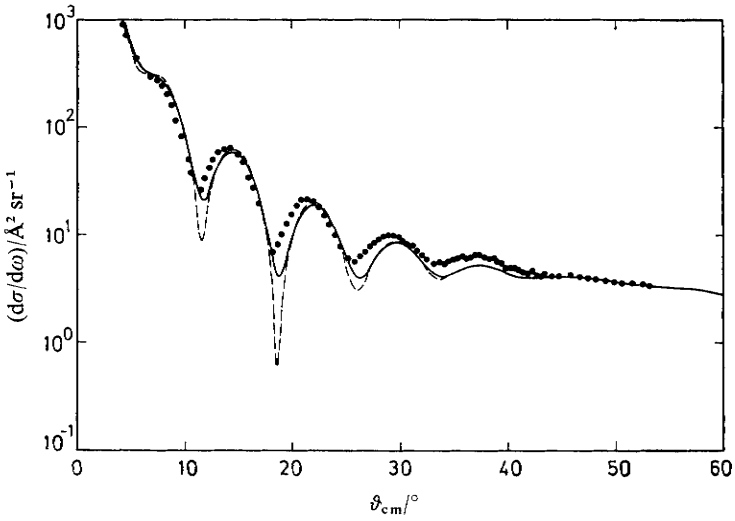

FIG. 8.—Effect of the angular and energy averaging by the present experiment. The (dashed line) theoretical total cross-section calculated for $E_{cm} = 27.3$ meV from the spherical KSK potential was convoluted with the apparatus $E_{cm} - \vartheta_{cm}$ weighting function, resulting in the (smooth line) convoluted cross-section. Comparison with the experimental total cross-section only (●) shows the KSK spherical potential is in similarly good agreement as was the full HTT potential in fig. 7.

of the minima, which is especially apparent for the first two very deep and sharp diffraction minima at $\vartheta_{cm} = 11.6$ and 18.3°. Only minor changes are, however, observed in the position and in the amplitude of the diffraction maxima which are decreased by the averaging of the present experiment by $<10\%$. Thus, the significantly larger deviations between the experiment and the model potential close-coupling cross-sections found in fig. 7 cannot be ascribed to the finite resolution of the experiment.

SENSITIVITY TESTS FOR VARIATIONS OF THE POTENTIAL

In order to estimate the magnitude of the errors in the model potential that could account for the remaining discrepancies between experiment and theory, a number of sensitivity test cross-section calculations were made with slightly changed potentials.

A first test has already been given in fig. 8 where the spherical $He–N_2$ potential of Keil, Slankas and Kupperman (KSK) and not the Habitz, Tang and Toennies (HTT) v_0 was used. As was seen in fig. 5 the KSK spherical potential is quite different from the v_0 term of the present potential model by a 7% smaller R_m. Because of the small v_2 term of the KSK potential, the (not shown) KSK rotational inelastic cross-sections are more than a factor of 5 too small. Nevertheless, as seen in fig. 8 the KSK effective

v_0 potential gives approximately the same fit to the experimental total cross-section points as did the close-coupling total cross-sections of the HTT potential in fig. 7. This seems to indicate that with strongly asymmetric potentials the total scattering cross-section structure is preferentially weighting the perpendicular orientation $V(R,\gamma = 90°) \simeq v_0(R) - \frac{1}{2} v_2(R)$ of the potential. As can be easily estimated from the HTT potential in fig. 5, this potential is quite close to the effective KSK v_0 potential.

Next, the influence of the non-spherical potential deformation on the inelastic cross-sections was checked. As already stated, the effect of the v_4 part of the potential on the experimentally observed $\Delta j = 2$ cross-sections is negligible. To see the influence of a change in the v_2 term the HTT potential model was shifted in R by an amount a: $v_2'(R) = v_2(R - a)$. The potential plots, fig. 9(*a*), show for $a = +0.08$,

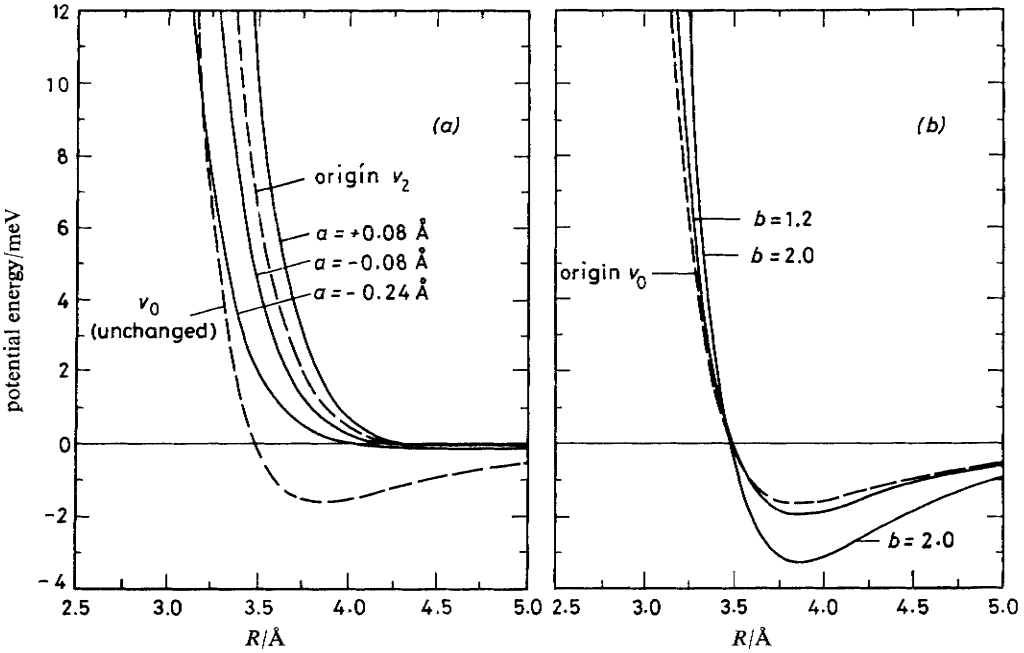

FIG. 9.—Variations of the HTT potential used for the sensitivity test calculations shown in the subsequent fig. 10 and 11. (*a*) $v_2'(R) = v_2(R - a)$; (*b*) $v_0'(R) = bv_0(R)$, v_2, v_4 omitted.

-0.08 and -0.24 Å how this produces slight right- or left-hand shifts of $v_2(R)$ and is thus increasing or decreasing the potential asymmetry. Fig. 10(*a*)-(*d*) compare the close-coupling total and $0 \rightarrow 2$ inelastic differential cross-sections obtained by these changes in v_2 with the respective experimental cross-sections of fig. 7. Fig. 10(*a*) shows that a shift of $v_2(R)$ by only $+0.08$ Å, *i.e. ca.* 2% of R_m, to larger R leads to a drastic (more than a factor of two) increase in the $0 \rightarrow 2$ cross-section and also to a noticeable shift in the locations of the diffraction pattern of the $0 \rightarrow 2$ as well as of the total cross-section. Shifts of $v_2(R)$ to smaller R by similar amounts of $a = -0.08$, -0.16 and -0.24 Å, shown in fig. 10(*b*)-(*d*), lead to a steady decrease of the $0 \rightarrow 2$ cross-section. For these decreasingly smaller aspherical deformations, however, the total cross-section remains nearly unaffected. In the $0 \rightarrow 2$ cross-section only the absolute magnitude is changed, but neither the overall structure nor the position of the maxima of the oscillations are effected. Thus, the experiment has been carried out under conditions where not only the ratio of the total to the inelastic cross-sections is chang-

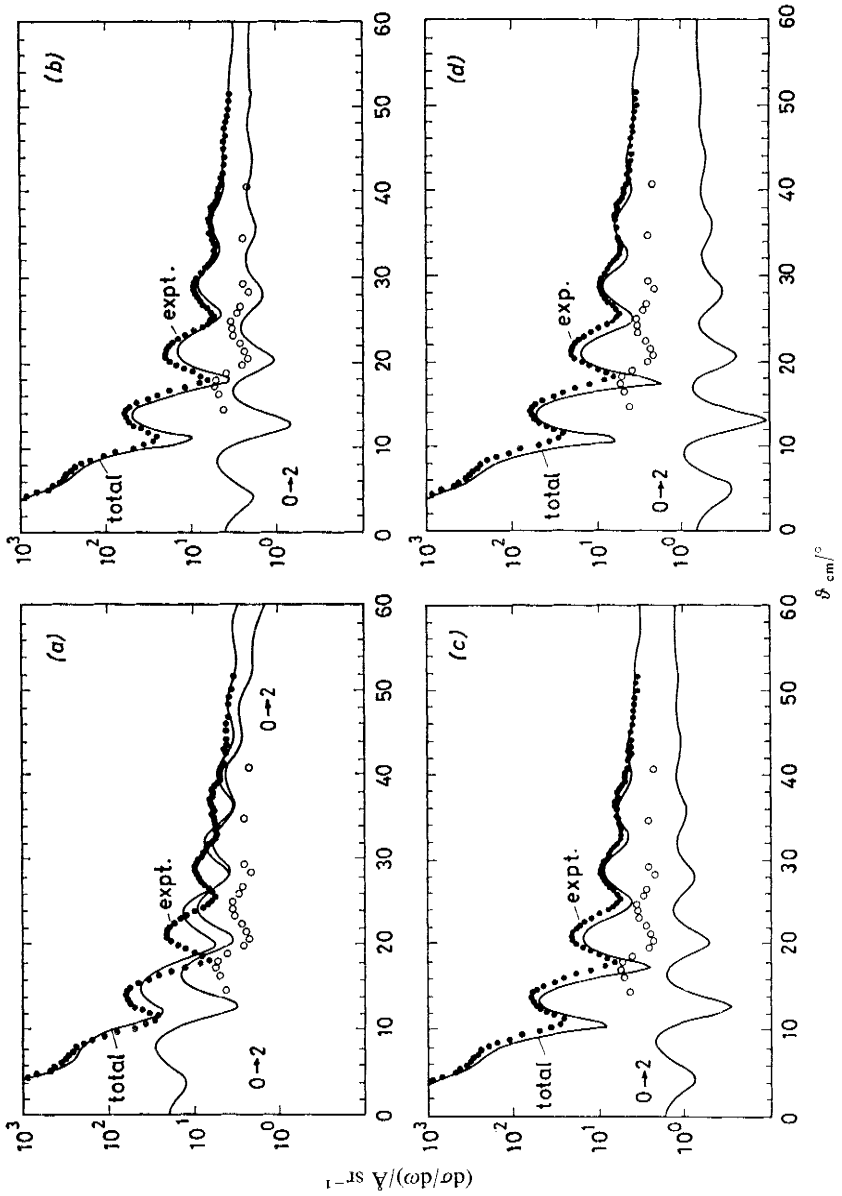

FIG. 10.—(*a*) to (*d*) show sensitivity test calculations of cross-sections for the v_2 potential term variations illustrated in fig. 9(*a*). (*a*) $a = +0.08$, (*b*) $a = -0.08$, (*c*) $a = -0.16$, (*d*) $a = 0.24$ Å. Smooth lines are the theoretical total and 0→2 rotational differential cross-sections, ● and ○ the respective experimental points. Compared with the changes induced in the theoretical 0→2 cross-section, the total cross-section is rather insensitive to these potential variations.

ing rapidly, but also the phase relation between the 0→2 and total differential cross-section undergoes rapid changes with small changes in the potential asymmetry.

The unexpected shift of the phase of the inelastic cross-sections at a critical potential deformation can be rationalized [16] from a consideration of the Fraunhofer diffraction from a ring-shaped aperture in a diaphragm.[24] Here, as in inelastic forward

scattering, only partial waves within an upper and lower bound can contribute to the diffraction. For this case a rather sudden transition occurs from the diffraction pattern of the full circular aperture (or equivalently a disc) to a similar but 180° phase-shifted pattern when the annular opening is made narrower than 20% of the outer radius.

Rather crude, but analytic, inelastic scattering models like the energy sudden inelastic Fraunhofer scattering theory for a slightly deformed hard sphere predict [25] that the rotationally inelastic cross-sections should be proportional to the square of the deformation amplitude δ. When assigning the deformation amplitude of this model to the difference of the repulsive potential $V(R,\gamma = 0)$ and the $V(R,\gamma = 90°)$ orientations (at 20 meV) the present value of the deformation would be $\delta = 0.6$ Å for the HTT–N_2 potential. A shift of $v_2(R)$ by $a = -0.24$ Å as used for the cross-section variation of fig. 10(*d*) reduces the deformation amplitude to $\delta' \approx 0.23$ Å, corresponding to a change of the original deformation $\delta = 0.6$ Å by a factor of 2.6. Thus, within the inelastic Fraunhofer model a reduction of the 0→2 cross-section by a factor of $(\delta/\delta')^2 = 6.8$ would be predicted, in good agreement with the close coupling result shown in fig. 10(*d*). From this δ^2 relationship, the amplitude deviation of *ca.* 15% between experimental 0→2 cross-section and the HTT potential prediction, fig. 7, would be removed by a maximal decrease of the deformation of only 7% to $\delta \approx 0.56$ Å, or, in terms of $v_2(R)$, by a shift of $a \approx -0.02$ to -0.03. The total cross-section, however, as is seen in fig. 10(*b*)-(*d*), would only be negligibly changed, and thus the discrepancy between the experimental and predicted total cross-section would remain.

Therefore, in a further sensitivity test calculation the v_0 term of the potential was changed by replacing $v_0(R) = bv_0(R)$. This variation of the v_0 potential, shown in fig. 9(*b*) for $b = 1.2$ and 2.0, linearly decreases the potential well without affecting seriously the location of the repulsive barrier. The effect on the total cross-section is shown in fig. 11, and is again compared with the experimental points. In relation to the dashed line cross-section from the HTT original v_0, $b = 1.2$ increases the total cross-section by

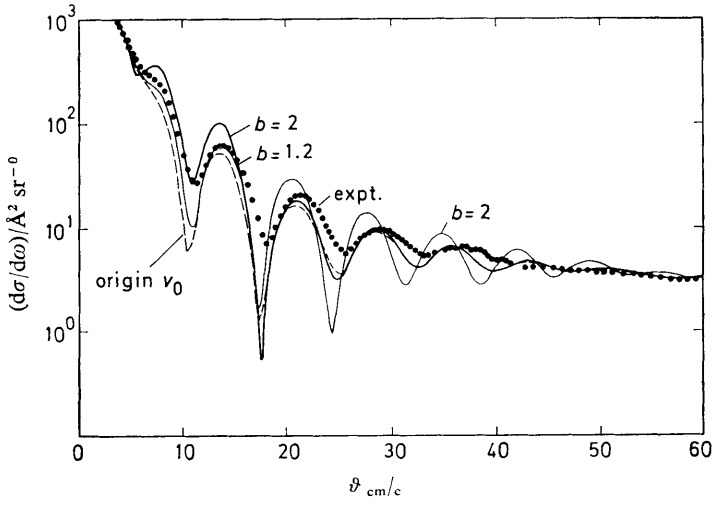

FIG. 11.—Sensitivity of the experimental (●) total differential cross-section to the v_0 part of the HTT potential. The v_0 potential term was varied as shown in fig. 9(*b*). The oscillation amplitude of the theoretical cross-sections (dashed for the original and smooth lines for the varied potential) increases when the parameter *b*, controlling essentially the well depth of the potential, is increased. $v_0'(R) = bv_0(R)$, v_2 and v_4 omitted.

approximately the right amount, and $b = 2.0$ gives too large an oscillation maxima. From this we estimate that the well depth of the present potential model is *ca.* 20% and at the very most 30% too shallow.

CONCLUSIONS

The comparisons between experimental cross-sections and calculations based on the potential of Habitz, Tang and Toennies reveal that the model provides an overall good description of the true potential. This agreement has been further substantiated by calculations of diffusion and viscosity coefficients,[26] which after account is taken of the relatively large anisotropy agree remarkably well ($<1\%$) with the published measurements.[27,28] The test provided by the differential cross-sections is an extremely critical one since the data is found to be sensitive to errors of only 0.02 Å in R and *ca.* 0.1 meV in energy in the potential-well region. The errors in the model potential are very small in the repulsive range but the well depth appears to be *ca.* 20% (≈ 0.3 meV) but definitely not more than 30% too shallow. In this connection it is gratifying to note that the model is based on estimated dispersion coefficients which were reduced by *ca.* 20% to bring them into agreement with the best semi-empirical previous estimates, and without this correction the model might well be in better agreement with experiment. Thus the agreement is roughly within the estimated errors of the input parameters of the model potential.

The present work indicates for highly anisotropic systems similar to He–N_2 that spherical potentials obtained from total cross-sections are quite different from the v_0 spherical term in the standard Legendre expansion. This is a striking departure from the experience for H_2 where the anisotropy is only a small perturbation and the experimental [29] and theoretical [30] evidence indicated that total cross-sections were only sensitive to v_0. However, the present study does suggest that it may be possible to generate good effectively spherical potentials which can account for the anisotropy and that such a potential possibly comes close to that for the most probable broadside approach. It remains to be seen if this rule holds for molecules where the potential is lowest for a collinear approach [31] for which the collision probability is less than for the broadside approach.

Another interesting generalization coming from the model potential is the observation that, just as found for H_2–rare-gas systems,[11] the reduced anisotropic potential $v_2(x_2)/\varepsilon_2$, where $x_2 = R/R_{m2}$, has the same form as the reduced isotropic potential $v_0(x_0)/\varepsilon_0$. This is quite remarkable when one examines the apparent big differences in the potentials, as shown in fig. 5. This suggests that the previously proposed law of corresponding isotropic and anisotropic potentials may have a general validity. This law has so far not been tested experimentally.

Now that the Tang–Toennies model has been found also to work well for He–N_2, the same frequency-dependent polarizabilities can be used to predict an anisotropic potential for Ne–N_2 and the important prototype system Ar–N_2 and eventually N_2–N_2 once the SCF calculations have been done. Work along these lines is in progress. The experiments, on the other hand, have been extended to He–O_2, CO, CH_4. With some apparatus improvements it should be also possible to study N_2–Ar and N_2–N_2.

We thank R. T. Pack (Los Alamos) and F. A. Gianturco (Rome) for many stimulating discussions, G. Drolshagen and A. Obst for help in carrying out some of the potential calculations and M. S. Bowers for calculations of transport properties. K. T. Tang thanks the National Science Foundation for grants CHE-7809808 and PRM-7921430 and the Research Corporation for additional funding.

[1] T. Kihara, *Intermolecular Forces* (Wiley, New York, 1978).
[2] J. O. Hirschfelder, C. F. Curtiss and R. B. Bird, *Molecular Theory of Gases and Liquids* (Wiley New York, 1954).
[3] J. Reuss, *Adv. Chem. Phys.*, 1976, **30**, 389.
[4] M. Faubel and J. P. Toennies, *Adv. At. Mol. Phys.*, 1977, **13**, 262.
[5] J. P. Toennies, *Discuss. Faraday Soc.*, 1962, **33**, 96.
[6] H. E. van den Bergh, M. Faubel and J. P. Toennies, *Faraday Discuss. Chem. Soc.*, 1973, **52**, 203.
[7] K. Rudolph and J. P. Toennies, *J. Chem. Phys.*, 1976, **65**, 4483; H. Schmidt, V. Hermann and F. Linder, *Chem. Phys. Lett.*, 1976, **41**, 365.
[8] U. Buck, F. Huisken and J. Schleusener, *J. Chem. Phys.*, 1978, **68**, 5654; W. R. Gentry and C. F. Giese, *J. Chem. Phys.*, 1977, **67**, 5389.
[9] K. T. Tang and J. P. Toennies, *J. Chem. Phys.*, 1977, **66**, 1496. For errata see *J. Chem. Phys.*, 1977, **67**, 375 and 1978, **68**, 786.
[10] R. Ahlrichs, R. Penco and G. Scoles, *Chem. Phys.*, 1977, **19**, 119.
[11] K. T. Tang and J. P. Toennies, *J. Chem. Phys.*, 1978, **68**, 5501 and 1981, **74**, 1148.
[12] K. T. Tang and J. P. Toennies, *J. Chem. Phys.*, to be published.
[13] M. Faubel, K. H. Kohl and J. P. Toennies, in *Rarefied Gas Dynamics*, ed. S. S. Fisher, *Prog. Astronaut. Aeronaut.*, 1981, **74**, 862.
[14] M. Faubel, K. H. Kohl and J. P. Toennies, *Book of Abstracts*, 12*th Int. Conf. Elect. At. Collisions*, ed. S. Datz (ORNL, Oakridge, Tennessee, 1981), p. 395.
[15] P. Habitz, K. T. Tang and J. P. Toennies, *Chem. Phys. Lett.*, 1982, **85**, 461.
[16] M. Faubel and E. R. Weiner, *J. Chem. Phys.*, 1981, **75**, 641.
[17] W. Meyer, *Chem Phys* , 1976, **27**, 27.
[18] P. Coulon, R. Luyckx and H. N. W. Lekkerkerker, *J. Chem. Phys.*, 1979, **71**, 3462.
[19] M. Keil, J. T. Slankas and A. Kuppermann, *J. Chem. Phys.*, 1979, **70**, 541.
[20] B. H. Choi and K. T. Tang, *J. Chem. Phys.*, 1975, **63**, 1775.
[21] D. Secrest, in *Atom-Molecule Collision Theory*, ed. R. B. Bernstein (Plenum Press, New York, 1979) chap. 8, p. 265-299.
[22] K. Bergmann, U. Hefter and J. Witt, *J. Chem. Phys.*, 1980, **72**, 4777.
[23] J. A. Serri, C. H. Becker, M. B. Elbel, J. L. Kinsey, W. P. Moskowitz and D. E. Pritchard, *J. Chem. Phys.*, 1981, **74**, 5116.
[24] M. Born and E. Wolf, *Principles of Optics* (Pergamon Press, Oxford, 6th edn, 1980), p. 417.
[25] J. S. Blair, in *Lectures in Theoretical Physics* (The University of Colorado Press, Boulder, 1966), vol. VIIIC, p. 343ff.
[26] M. S. Bowers and K. T. Tang, to be published.
[27] J. Kestin, S. T. Ro and W. A. Wakeham, *J. Chem. Phys.*, 1972, **56**, 4036.
[28] P. S. Arora and P. J. Dunlop, *J. Chem. Phys.*, 1979, **71**, 2430.
[29] A. Kuppermann, R. J. Gordon and M. T. Coggiola, *Faraday Discuss. Chem. Soc.*, 1973, **55**, 145.
[30] P. McGuire, *Chem. Phys.*, 1974, **4**, 483.
[31] G. Ewing, *Annu. Rev. Phys. Chem.*, 1976, **27**, 553.